A Deterministic VOR Error Modelling Method – Application to Wind Turbines

Ludovic Claudepierre, Rémi Douvenot, Alexandre Chabory, Christophe Morlaas

A Deterministic VOR Error Modelling Method – Application to Wind Turbines.

Ludovic Claudepierre, Rémi Douvenot, Alexandre Chabory, and Christophe Morlaas.

***Abstract*—VOR devices are sensitive to multipath. These perturbations yield an error on the azimuth information received by the aircraft. This article presents a simulation method to estimate the impact of the environment on the received VOR signal. This method uses a two-ray model and a hybridisation between parabolic equation (PE) and physical optics (PO). The direct field between the VOR station and the aircraft is given by a two-ray model, PE is used to compute the propagation between the VOR station and the obstacles, and PO is used to compute the scattered field. Finally, the VOR error is deduced from the direct and the scattered fields. The hybridisation between PE and PO is performed as follows: the obstacles are meshed and the PE incident field is cast as a plane wave on each facet to efficiently compute the scattered field. The simulation method is confronted to in-flight measurements in the presence of a wind farm around a VOR station in Boulogne-sur-Mer, France. The maximum VOR error along the trajectories is retrieved within 1.1 degree and the statistical behaviour is reproduced. The standard deviation is within 0.3 degree, and the skewness and Kurtosis differ of less than 2 between simulations and measurements. Finally, parametric studies performed with this method show that the rotor-blades can be neglected in this scenario. It is also shown that the knowledge of the aircraft trajectory is of major importance to predict or reproduce VOR error measurements.**

***Index Terms*—VHF devices, computational electromagnetics, multipath channels, radiowave propagation, wind farms.**

I. Introduction

VHF Omnidirectional Range (VOR) devices are essential for the navigation of aircraft. Used as radio beacons, they give their bearing, *i.e.* their heading with respect to the magnetic North. A VOR station transmits two horizontally-polarised signals denoted as REF (reference) and VAR (variable). The latter depends on the bearing. These signals are either amplitude or frequency modulated. In conventional VOR (CVOR), the REF is phase modulated and the VAR is amplitude modulated. For Doppler VOR (DVOR), the modulations are reversed.

In the absence of an obstacle, the field between the VOR station and the aircraft can be easily calculated using a two-ray model [1]. However, nearby obstacles yield multipath. Consequently, these parasite signals have to be accurately quantified in order to predict issues on the bearing information.

Building erection in the close vicinity of the civil aviation systems requires an approval from the civil aviation authority. In Europe, official recommendations are based on a geometrically-defined building restricted area (BRA) [2]. Nevertheless, these recommendations are very restrictive. In practice, every country applies its own specific rules on the tolerated bearing error. For example, in France the error must be smaller than 3° on 95 % of the flight inspection measurements and never exceed 3.5°.

In order to evaluate the scatterers impact on the VOR signals, electromagnetic simulations are required. In particular, the VOR receiver model needs an accurate determination of the amplitude, phase, and direction of arrival of the scattered fields [3]. Among the different scattering objects potentially erected nearby a VOR station, wind turbines are a common concern for civil aviation. Accurate results on that type of structure are usually time and memory intensive [4], which prevent any parametric study. Thus, the method has to reach a compromise between accuracy of the result and time requirement. Note that the term "scattering" used in this article denotes the fields radiated by scatterers, notably reflection and diffraction.

In literature, methods using the wind turbine radar cross section (RCS) have been proposed by De la Vega *et al.* [5]. The authors calculate the intersection between the second Fresnel ellipsoid and the obstacle from which they deduce areas of strong and weak impact. Calo Casanova *et al.* [6] have used a similar method with the wind turbine reflection coefficient from the ITU recommendation [7]. Areas where the perturbations are maximum can be delimited. These 2 methods are fast but use coarse approximations on the scattering calculation. Morlaas *et al.* [4] have proposed to compute the wind turbine RCS by the method of moments (MoM). The VOR error is then computed with the analytic expression proposed by Odunaiya *et al.* [3]. This method is accurate in terms of scattering computation. Nevertheless, the RCS has to be computed for every type of wind turbine. More recently, Fernandes *et al.* [8] have proposed to use the knife-edge model to take into account the relief. This latter method is fast at the cost of a loss of accuracy. The combination of ray-tracing and the uniform theory of diffraction has also been proposed [9]. This method accounts for multiple reflections and diffractions. Another method is the hybridisation between MoM and Physical Optic (PO) presented by González *et al.* [10]. Both are accurate but also memory intensive for complex scenarios. Finally, hybridisations between parabolic equation (PE) and PO have been proposed by Morlaas *et al.* [11] and Calo Casanova *et al.* [12]. These methods present a good compromise between accuracy and time requirement.

In this paper, an efficient hybridisation between PE and PO is detailed and tested. For the sake of conciseness, this hybridisation is denoted as PEPO in the following. In addition,

The authors are with ENAC, TELECOM/EMA, F-31055 Toulouse, France and Toulouse University, F-31400 Toulouse, France.
E-mail: douvenot@recherche.enac.fr
Manuscript received month XX, 201X

after the overall presentation of this method, the simulation results are compared with two sets of in-flight inspection measurements around a CVOR station in Boulogne-sur-Mer (France). To our knowledge, such a comparison has never been published previously. The likeness between the simulated and the measured VOR errors in terms of maximal error and statistical moments up to order 4 is presented to show the interest of the simulation method. Afterwards, the PEPO method is used to emphasise the high variability of the error with the aircraft trajectory.

This paper is organised as follows. Two-ray model, PE, PO, and hybridisation are presented in Section II with the VOR receiver model. In Section III, the method is tested through comparisons with flight inspection measurements in Boulogne-sur-Mer (France) in the presence of wind turbines. Section IV introduces a parametric study to highlight that the differences between the flight measurements mainly come from the differences in the measurement trajectories. A summary of this work is provided in Section V with leads for future improvements.

II. Presentation of the Method

A. Overview of the PEPO Method

The PEPO method hybridises three methods (Figure 1). The field from the VOR station to the aircraft is calculated with a two-ray model [1]. The fields from the VOR station to the scatterers are simulated with PE. Then, the scattered fields are computed by PO. The scattered and the direct fields are combined to calculate the VOR error. The block diagram is displayed in Figure 2. The following inputs are given: coordinates and radiation pattern of the VOR station antenna, coordinates and geometry of the obstacles, coordinates of the observation points, and relief. Afterwards, the incident fields on the obstacles are computed by PE. In this step, the incident field is calculated for every obstacle without considering the interaction between them because at the VOR frequency and for wind turbines, the shadowing effect can be neglected as validated in [13].

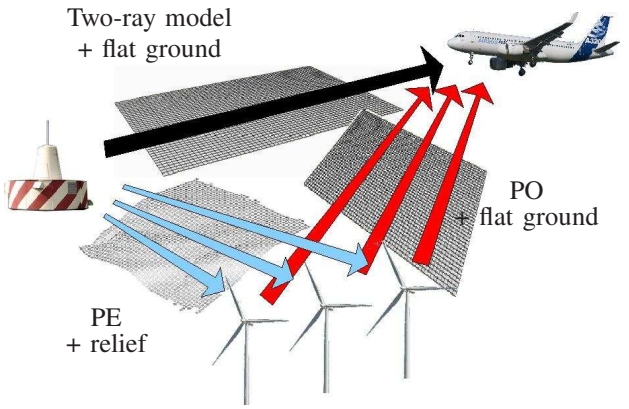

Figure 1: Overview of the method.

The incident fields are then interpolated on a polygonal mesh of the obstacles to obtain equivalent currents under the PO assumptions. These currents are calculated for scatterers either metallic or composed of dielectric slabs. Once the currents on each obstacle are known, the scattered fields are computed on the observation points considering a flat dielectric ground. Finally, the direct field is combined to the scattered fields to obtain the VOR error. This method can be performed on a standard computer in reasonable time and with a good accuracy. This allows to perform multiple parametric studies, for example to test several configurations of a wind farm. Moreover, the main output of the method is the VOR error, which can easily be interpreted by air transport authorities. Note that PEPO is valid for any type of scatterer for which the PO approximation holds.

Several hypotheses are made in the PEPO method. Two of them are specifically discussed here. First PE is only used between the VOR station and the scatterers. PE could also be used from the VOR station to the obstacle (direct field), from the obstacle to the aircraft (scattered field) and from the VOR station to the aircraft (direct field) as proposed in [12] to consider the relief. The computation time of PE increases with the vertical domain size in $N_z \log N_z$ with N_z the number of vertical points. The vertical domain should correspond to the flight altitude for the direct and the scattered fields. Thus it would be time-intensive to use PE in these two areas. In the case of scatterers close to the VOR station, the trajectory from the VOR station to the aircraft and from the obstacle to the aircraft are similar. Moreover, the VOR error depends on the ratio between the scattered and direct fields, and the relief is accounted in the same way on these two signals. Finally, as proposed in [11], PE is only used between the VOR station and the scatterer.

The receiver model is static. This assumption needs to be discussed. Indeed, the rapidly rotating blades and the moving aircraft induce a Doppler effect on the scattered field. Nevertheless, unlike at radar frequencies, the blades must be considered dielectric at VOR frequency, which reduces their contribution in the total scattered field [14]. Moreover, Morlaas *et al.* [4] have shown that the Doppler shift effect on the envelop of the VOR error is negligible. So, this static receiver model can be used for VOR error modelling in the presence of wind turbines.

B. VOR to Aircraft Propagation: Two-Ray Model

The direct electromagnetic field radiated by the VOR antenna is calculated at a point $\boldsymbol{r} = (r,\, \theta,\, \varphi)$ in the spherical coordinates system centred on the VOR station. The two-ray model [15] that takes into account a flat dielectric ground by considering both the actual and the image sources is used.

First, the horizontally polarised electric field $\boldsymbol{E}_{\text{FS}}$ from the actual antenna, calculated in free-space and oriented along $\hat{\boldsymbol{\varphi}}$ is expressed as

$$\boldsymbol{E}_{\text{FS}}(\boldsymbol{r}) = \sqrt{\frac{\zeta_0 P_{\text{ant}}}{2\pi} G_{\text{ant}}} \frac{e^{j(\theta_{\text{ant}} - k_0 r)}}{r} \hat{\boldsymbol{\varphi}}, \tag{1}$$

with ζ_0 the vacuum impedance, k_0 the wavenumber, and P_{ant} the power provided to the antenna. G_{ant} and θ_{ant} are the gain and the phase of the radiation pattern of the VOR antenna in the direction of observation.

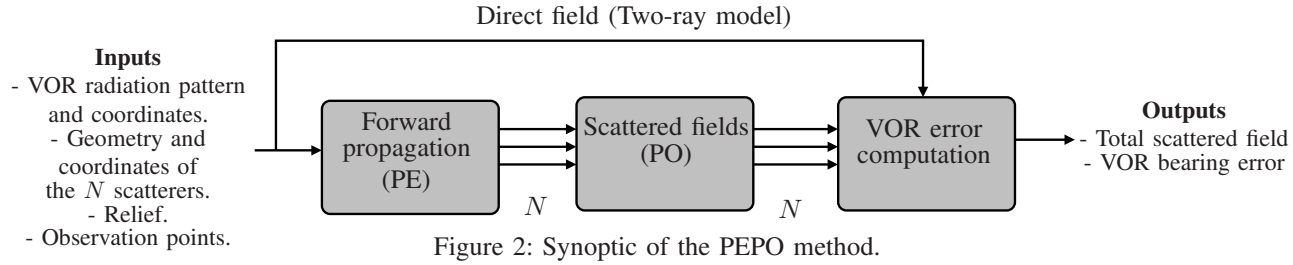

Figure 2: Synoptic of the PEPO method.

In the presence of the ground, the electromagnetic field radiated by the image source $\boldsymbol{E}_{\text{im}}$ is computed similarly [1]. Thus, the direct field is given by

$$\boldsymbol{E}_{\text{dir}} = \boldsymbol{E}_{\text{FS}} + \Gamma \boldsymbol{E}_{\text{im}}, \tag{2}$$

where Γ is the Fresnel reflection coefficient of the ground considered as dielectric with finite conductivity. The reflection coefficient for the horizontal polarisation is given by

$$\Gamma = \frac{k_{0z} - k_{\text{g}z}}{k_{0z} + k_{\text{g}z}}, \tag{3}$$

where k_{0z} and $k_{\text{g}z}$ are the vertical components of the wavenumbers of the incident and transmitted waves, respectively. They are given by $k_{0z} = k_0 \cos\theta_{\text{i}}$ and $k_{\text{g}z} = \sqrt{k_{\text{g}}^2 - k_0^2 \sin^2\theta_{\text{i}}}$, with k_0 and k_{g} the wavenumbers in the atmosphere and in the ground, and θ_{i} the angle of incidence. The ground permittivity used to define k_{g} is complex and includes the conductivity.

The two-ray model is used to compute the direct field received by the aircraft from the VOR station.

C. VOR Station to Scatterers: Parabolic Equation

PE is used to calculate the electromagnetic propagation between the VOR station and the scatterers because of its robustness and accuracy in the presence of irregular and dielectric grounds [16]. Moreover, the radiation pattern of the antenna is taken into account. The cylindrical coordinates (ρ, φ, z) centred on the VOR station are used.

PE is a forward 2D propagation method. Therefore, the scene is considered invariant by rotation around the $\hat{\boldsymbol{z}}$ axis and the backward propagation is neglected.

From the 2D Helmholtz equation, these approximations and the introduction of the reduced variable $u = E_\varphi \sqrt{\rho} e^{jk_0\rho}$ lead to the standard PE valid for small angles around the paraxial direction given by [17]

$$\frac{\partial u}{\partial \rho} = -\frac{jk_0}{2}\left(\frac{1}{k_0^2}\frac{\partial^2 u}{\partial z^2} + (n^2 - 1)u(\rho, z)\right), \tag{4}$$

where n is the refractive index.

The split-step Fourier formulation is applied to solve this equation iteratively [18]. The propagation is performed in the spectral domain whereas the atmosphere is considered in the spatial domain. Expression (4) is finally solved by

$$\begin{aligned} u(\rho + \Delta\rho, z) = \exp\left(-\frac{jk_0(n^2-1)\Delta\rho}{2}\right) \\ \times \mathcal{F}^{-1}\left[\exp\left(\frac{jk_z^2\Delta\rho}{k_0}\right)\mathcal{F}\left(u(\rho, z)\right)\right], \end{aligned} \tag{5}$$

where k_z is the z component of the wavevector corresponding to the spectral variable and $\Delta\rho$ is the horizontal step for the propagation. $\mathcal{F}$ and $\mathcal{F}^{-1}$ denote the Fourier transform and inverse Fourier transform, respectively.

In this split-step method, the propagation is applied in two steps. First, the propagation through a homogeneous atmosphere is applied in the spectral domain. Second, a phase screen is applied to take into account the refractive index in the space domain. At this step, the relief is accounted by a staircase modelling that is accurate for moderate slopes [16]. The Discrete Mixed Fourier Transform [18] is used here. It is an efficient and stable numerical scheme for the Fourier transform in the presence of ground reflections.

To take into account the dielectric behaviour of the ground, the Leontovich impedance boundary condition is considered [19]. The ground roughness can be easily accounted by modifying the reflection coefficient Γ [20]. At the top of the computation domain, a hyperbolic tangent apodisation is applied.

The advantages of simulating the electromagnetic wave in this area with PE are many. PE takes into account the radiation pattern of the VOR antenna and accurately considers the relief, the ground composition, and its roughness. In particular, a multilayer ground can be considered, to model a snow layer for example.

On the other hand, this method implies a 2D approximation. This classical approximation for moderate reliefs neglects the scattering by side relief. Except for very mountainous environments, this approximation is relevant and extensively used [16], [12]. In the case of a sharp relief, the validity of the azimuthal invariance could be questioned. The other limitations of PE have no consequence since the scatterers are in the paraxial cone of validity [18], and the neglected backscattered wave is of no interest here.

The amplitude and the phase of the fields are both important in the calculation of the VOR error [3]. Therefore, the grid size $\Delta\rho$ and Δz are chosen so as to obtain an accuracy of 0.5 dB in amplitude and 3° in phase. These criteria ensure a good accuracy on the VOR error since the field scattered by the obstacles is in itself weaker than the direct field (typically at least 10 dB weaker).

D. Incident Fields on the Scatterers: Hybridisation

To perform an efficient computation of the fields radiated by the induced currents on each facet, the incident field is locally represented as a plane wave. This can be achieved by taking a sufficiently fine mesh such that the equivalent current on one facet has a constant magnitude and a linear phase. This

method can be applied for metallic or multilayer dielectric slabs. A simplified model for the multilayer blades of the wind turbines is used [14].

The incident field being a plane wave, it is entirely described by its amplitude, its phase, its polarisation, and its direction of propagation. The hybridisation between PE and PO consists in the characterisation of this incident plane wave on each facet.

The cylindrical coordinates are used here. The incident field is computed by PE on a vertical axis that is commonly the central axis of the obstacle. The direction of incidence of the field on the n^{th} facet is given by its wavevector. The vertical component k_{zn} is obtained by a linear interpolation of the phase of the incident field whereas the radial component of the wavevector $k_{\rho n}$ is calculated as

$$k_{\rho n} = \sqrt{k_0^2 - k_{zn}^2}. \tag{6}$$

The incidence direction on the n^{th} facet is finally deduced from

$$\hat{\boldsymbol{s}}_n = \frac{k_{\rho n}\hat{\boldsymbol{\rho}} + k_{zn}\hat{\boldsymbol{z}}}{k_0}. \tag{7}$$

Let $\boldsymbol{b}_n$ be the barycentre of the n^{th} facet. The incident field is first interpolated at the same altitude as $\boldsymbol{b}_n$. Then, a phase shift is applied on the field to account for the radial distance between $\boldsymbol{b}_n$ and the central axis of the obstacle. Thus, the incident field on each facet is obtained.

E. Scatterers to Aircraft: Physical Optics

As the incident field $(\boldsymbol{E}_{\text{i}}, \boldsymbol{H}_{\text{i}})$ is a plane wave, the electric and magnetic currents on the n^{th} facet have constant magnitudes and linear phases. Moreover, the reflection and transmission coefficients can be calculated from the material characteristics to deduce the reflected field $(\boldsymbol{E}_{\text{r}}, \boldsymbol{H}_{\text{r}})$ and the transmitted field $(\boldsymbol{E}_{\text{t}}, \boldsymbol{H}_{\text{t}})$ at the interfaces. Then, the complex amplitudes of the currents $\boldsymbol{J}_n$ and $\boldsymbol{M}_n$ at $\boldsymbol{b}_n$ are given by

$$\begin{aligned} \boldsymbol{J}_n &= \hat{\boldsymbol{n}}_n \times (\boldsymbol{H}_{\text{i}}(\boldsymbol{b}_n) + \boldsymbol{H}_{\text{r}}(\boldsymbol{b}_n) - \boldsymbol{H}_{\text{t}}(\boldsymbol{b}_n)), \\ \boldsymbol{M}_n &= -\hat{\boldsymbol{n}}_n \times (\boldsymbol{E}_{\text{i}}(\boldsymbol{b}_n) + \boldsymbol{E}_{\text{r}}(\boldsymbol{b}_n) - \boldsymbol{E}_{\text{t}}(\boldsymbol{b}_n)), \end{aligned} \tag{8}$$

where $\hat{\boldsymbol{n}}_n$ is the vector normal to the surface at the point $\boldsymbol{b}_n$.

The far-field radiation integrals [1] are used to express the electric field $\boldsymbol{E}_n$ scattered by the current on facet n. The constant complex amplitudes $\boldsymbol{J}_n$ and $\boldsymbol{M}_n$ of the electric and magnetic currents densities on the n^{th} facet are put out of the integral. Only the linear phase term remains. One obtains

$$\begin{aligned} \boldsymbol{E}_n(\boldsymbol{r}) = \frac{jk_0\zeta_0}{4\pi}\hat{\boldsymbol{r}}_n \times (\hat{\boldsymbol{r}}_n \times \boldsymbol{J}_n + \boldsymbol{M}_n)\frac{e^{-jk_0 r_n}}{r_n} \\ \iint_{S_n} e^{-jk_0(\hat{\boldsymbol{s}}_n - \hat{\boldsymbol{r}}_n)\cdot(\boldsymbol{r}' - \boldsymbol{b}_n)} d\boldsymbol{r}', \end{aligned} \tag{9}$$

where S_n is the surface of the n^{th} facet, ζ_0 is the free-space impedance, and $\boldsymbol{r}_n = r_n\hat{\boldsymbol{r}}_n$ is the vector from the barycentre of the n^{th} facet $\boldsymbol{b}_n$ to the observation point $\boldsymbol{r}$. This equation is valid in the far-field of the facets.

The phase integral in (9) has a closed-form formulation [21] obtained from the Fourier transform of polygonal shape functions [22]. The ground, considered as a perfect plane is taken into account using the image theory [1]. The ground reflection coefficient includes the complex permittivity and the conductivity of the surface. The method has been validated for wind turbines at VOR frequency in [11], [14].

The contribution of lightning-rods in wind turbine blades is taken into account by means of a canonical RCS expression [23].

F. VOR Error Computation

The VOR error is the bearing error due to multipath at the output of the demodulator.

In a previous step, the fields scattered by each facet are clustered with respect to their azimuth of arrival. The amplitude and phase of the direct and multipath signals are calculated at the receiver considering that the on-board antenna is omnidirectional and horizontally polarised.

The VOR error is then obtained by combining the multipath with the direct signal according to Odunaiya and Quinet [3]. For a CVOR, the error ε^{c} is given by

$$\varepsilon^{\text{c}} = \tan^{-1}\left(\frac{-\sum_{n=1}^{N} a_n \cos(\theta_n)\sin(\varphi_n)}{1 + \sum_{n=1}^{N} a_n \cos(\theta_n)\cos(\varphi_n)}\right), \tag{10}$$

where a_n, θ_n, and φ_n are the amplitude, phase, and azimuth of the n^{th} multipath, respectively. They are relative to the amplitude, phase, and azimuth of the direct field. The error for the DVOR can be described by another expression with the same inputs [3].

This calculation does not take into account the dynamic effects due to mobile scatterers and aircraft.

III. Comparison with Measurements

A. Measurement Campaign

The case of 9 wind turbines ENERCON E-70 erected around the CVOR of Boulogne-sur-Mer (France) at the frequency of 113.8 MHz is studied (Figure 3). They are placed along 3 different azimuths (0° is towards East). These azimuths and their distances from the VOR station are presented in Table I. The reliefs between the VOR station and the wind turbines are given in Figure 4.

These wind turbines, represented by yellow circles in Figure 3, are composed by a metallic conic mast (height = 98 m, top diameter = 2 m, and bottom diameter = 7.5 m), a hub modelled by a metallic rectangular parallelepiped ($4 \times 11 \times 4$ m^3), and 3 blades (length = 35 m) modelled by 2 parallel dielectric slabs (spar with $\epsilon_r = 5$ and thickness = 44 mm) with a metallic rod (lightning protection with diameter = 10 mm) between

Azimuth	VOR - wind turbine distances (m)		
$-1°$	4402	4674	4978
$-22°$	3540	3839	4144
$-40°$	4437	4674	4920

Table I: Polar coordinates of the 9 wind turbines studied at Boulogne-sur-Mer. There are 3 wind turbines per azimuth.

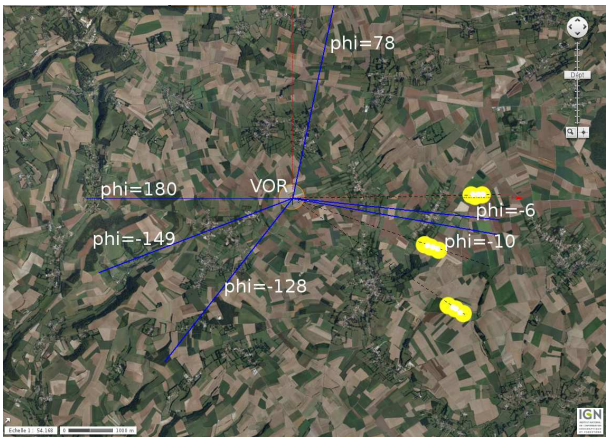

Figure 3: Wind farm at 5 km from the CVOR of Boulogne-sur-Mer (France) and measured azimuths (Source: Géoportail).

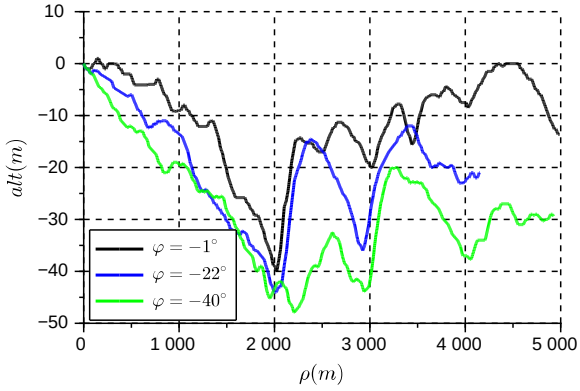

Figure 4: Relief profiles (relative to the VOR station altitude) between the VOR station and the wind turbines along the three different azimuths.

them. This wind turbine model has been validated under the PO approximations in [14].

During the flight tests, the VOR error has been measured on six azimuths (blue lines in Figure 3) around the VOR in three different configurations corresponding to three different dates:

- no wind turbines within 15 km around the VOR station (May 2009);
- the 9 wind turbine masts at less than 5 km from the VOR station, see Table I (July 2012);
- the 9 complete wind turbines at less than 5 km (November 2012).

Only the measurements on the azimuths $\varphi = -10°$ and $\varphi = -6°$ are presented here. These azimuths are the most relevant to test our method since the error due to the wind turbines exceeds the residual error already present without the wind turbines. The observation points are measured by an on-board GPS receiver and the exact orientations of the hubs are known.

The results of the three measurements campaigns on the azimuths $\varphi = -10°$ and $\varphi = -6°$ are plotted in Figure 5. A residual error with peaks as strong as $1°$ already exists without the wind turbines. This is of the same order as the error due to the wind turbines in the first 15 NM. This residual error can be explained by the presence of other scatterers and noise in the system. After 15 NM, the error due to the wind turbines is preponderant and the measurements are used for testing the PEPO method.

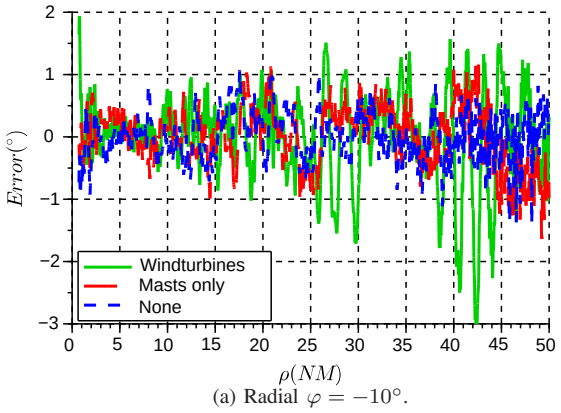

(a) Radial $\varphi = -10°$.

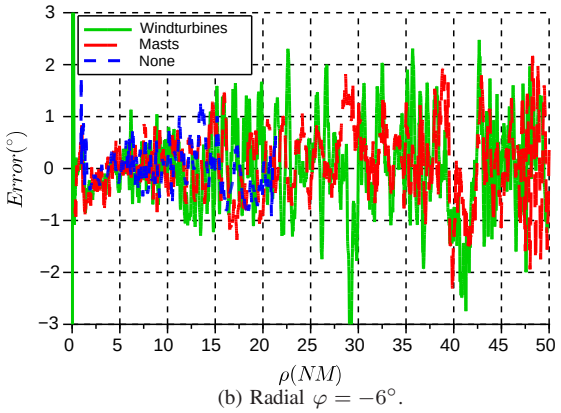

(b) Radial $\varphi = -6°$.

Figure 5: Measured VOR error with respect to distance for the three campaigns and on the two azimuths $\varphi = -10°$ and $\varphi = -6°$.

The oscillations visible in the green plot of Figure 5 between 25 and 30 NM and between 40 and 45 NM are due to the recombination of signals which relative phases varies from constructive to destructive interference. This phenomenon is denoted as scalloping [24]. The exact position of the maxima and minima of the scalloping are almost impossible to predict because they imply the knowledge of all the scatterers positions with an accuracy of typically $\lambda/8$. Also, scalloping is not always visible on the data because 9 main scatterers are involved, which implies complex signal recombinations.

Consequently, the order of magnitude of the measured VOR error and its statistical behaviour are expected to be reproduced by the simulation method rather than the exact positions of the maxima and minima.

The flight altitudes and the azimuths of the aircraft trajectories with respect to the distance from the VOR station are plotted in Figures 6 and 7, respectively. The receiver

trajectories are slightly different on the three measurement campaigns for the same radial, in both altitude and azimuth. The differences between the measured VOR error with masts only and with the wind turbines are mainly due to the azimuth variation as explained in sections IV-A and IV-B.

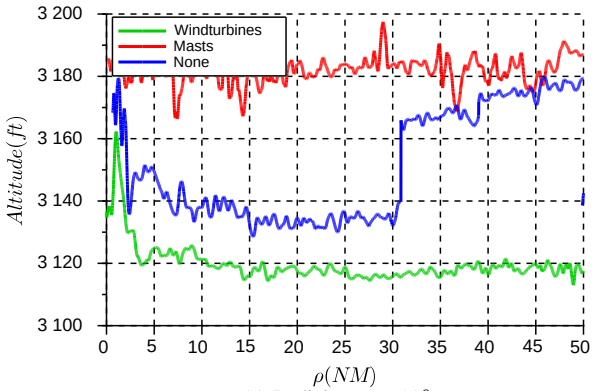

(a) Radial $\varphi = -10°$.

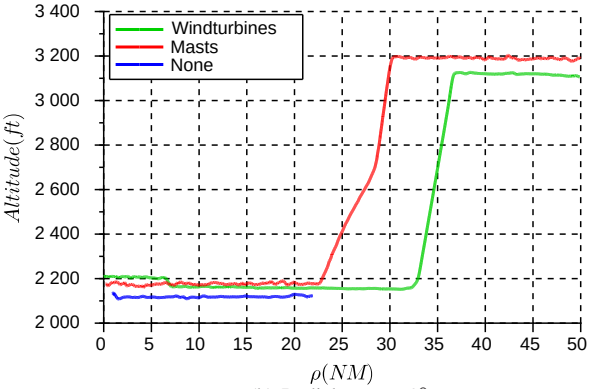

(b) Radial $\varphi = -6°$.

Figure 6: Flight altitude of the aircraft for the three measurement campaigns on the azimuths $\varphi = -10°$ and $\varphi = -6°$.

B. Simulation Results

For the PE simulations, the ground is considered as a homogeneous dry ground ($\epsilon_r = 25$, $\sigma = 0.02$ S.m^{-1} [25]). The horizontal step is 50 m and 256 points are taken on the 200 m of altitude. These values are typical at this frequency and for a moderate relief [26]. Figure 8 gives the 2D electromagnetic field normalised with distance computed with PE between the VOR station and the wind turbine at azimuth 1° and distance 4402 m from the VOR (see Table I). This illustrates that the relief is important in the modelling. The two-ray model considers the same ground composition.

The mesh strategy used for PO follows three criteria. First, to ensure that the incident field can be assimilated to a plane wave on each facet, the maximal variation of the amplitude on each one must not exceed 10 %. Second, a minimum of 8 facets is used to describe a circle. Finally, if the observation points are not in the far field of each facet, the mesh is refined.

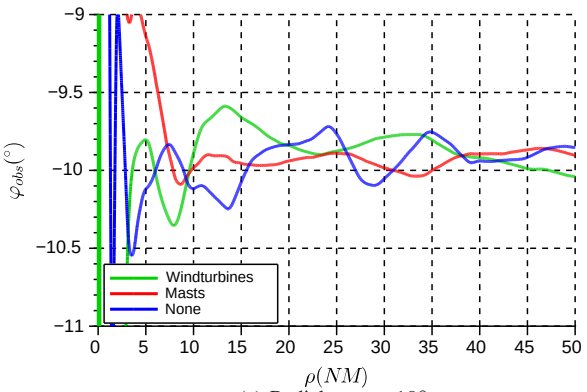

(a) Radial $\varphi = -10°$.

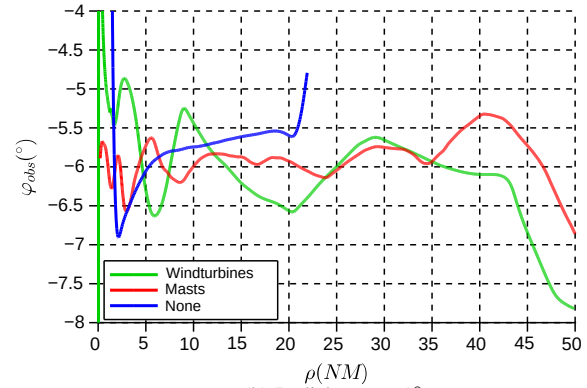

(b) Radial $\varphi = -6°$.

Figure 7: Azimuth of the aircraft for the three measurement campaigns on the azimuths $\varphi = -10°$ and $\varphi = -6°$.

In this configuration, the VOR error is simulated with the PEPO method for the 4 scenarios: with and without the wind turbine blades, and on azimuths $-10°$ and $-6°$.

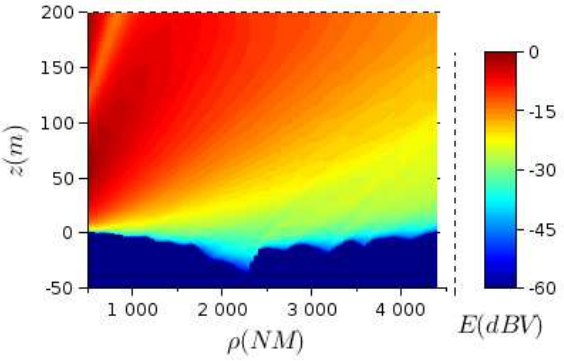

Figure 8: Electromagnetic field normalised in distance computed by PE from the VOR station to the wind turbine 1. The relief is in dark blue.

Figures 9a and 9b give the simulated and measured VOR error due to the mast during the July 2012 campaign for $\varphi = -10°$ and $\varphi = -6°$, respectively. Figures 10a and 10b give the VOR error due to the complete wind turbines

during the November 2012 campaign with respect to distance on the azimuths $\varphi = -10°$ and $\varphi = -6°$, respectively. We remind that the aircraft trajectory varies with the measurement campaign.

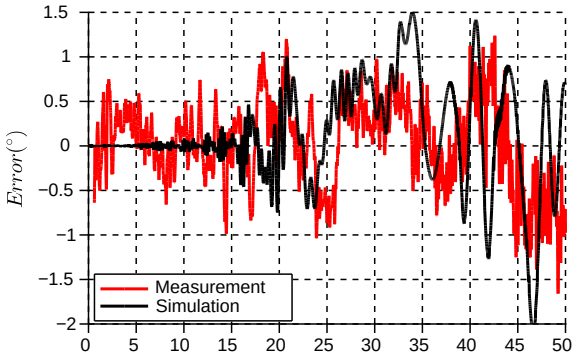

(a) Radial $\varphi = -10°$.

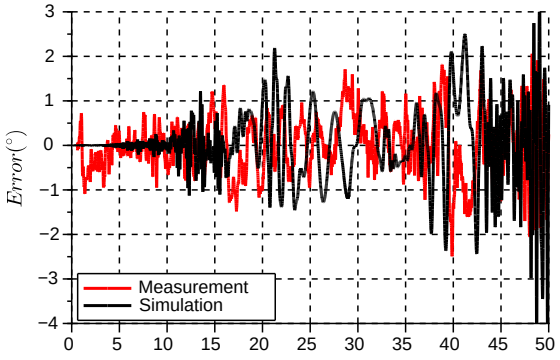

(b) Radial $\varphi = -6°$.

Figure 9: Measured and simulated VOR error with respect to distance in the presence of the masts (July 2012) along two azimuths.

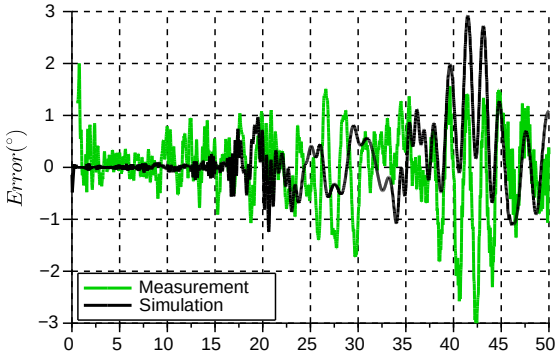

(a) Radial $\varphi = -10°$.

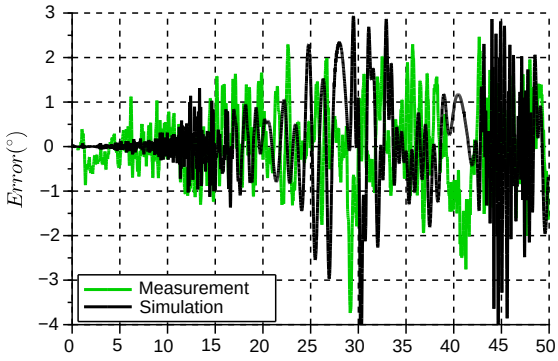

(b) Radial $\varphi = -6°$.

Figure 10: Measured and simulated VOR error with respect to distance in the presence of the wind turbines (November 2012) along two azimuths.

First, in Figures 9 and 10, the aforementioned residual error is visible from 0 to 15 NM. Between 15 to 50 NM, the global behaviour of the VOR error is retrieved: the error envelop globally matches, and the main oscillations are retrieved.

The behaviour of the results are quantified by their maxima and their statistical moments [27]. The second moment corresponds to the standard deviation. The skewness and the Kurtosis are the third and fourth moments normalised by the standard deviation, respectively. Skewness gives the symmetry of the distribution whereas Kurtosis denotes here the excess Kurtosis, *i.e.* the flatness of the data distribution compared to the Gaussian distribution. Skewness and Kurtosis differences smaller than 2 between two distributions are generally used to denote a good agreement [28].

Beforehand, a data processing step is performed: a low-pass filter is applied to remove the noise and the data are bounded between 15 and 50 NM. An example of processed data is shown in Figure 11. Then the moments are calculated.

Table II gathers the maximum error and the studied moments for the four measurements and the corresponding simulations. The maxima obtained by simulations are of the same order as the measurements, the difference being always smaller to 1.1°. In Figures 9 and 10, the maxima in the measurements correspond to maxima in the simulations. Therefore, the maxima are localised with the correct order of magnitude. Note that the maximum errors obtained by simulation are larger or equal to than the measured ones. This could be expected since the extreme values are usually reduced during measurements because of the complex environment.

For the same reason, simulations slightly overestimate the standard deviations. However, the differences between simulated and measured standard deviations are smaller than $0.3°$, which shows that the dispersion around the mean value is in the same order.

The skewness and the Kurtosis of the measurements and simulations are also in good agreement (differences smaller than 2). The skewness is close to zero for all the data, which denotes a symmetrical dispersion of the error between positive and negative values. The Kurtosis is generally slightly larger than 0, which implies a distribution slightly more peaky than a Gaussian.

Finally, considering that the maxima and statistical be-

Campaign	July 2012				November 2012			
Azimuth	$\phi = -6°$		$\phi = -10°$		$\phi = -6°$		$\phi = -10°$	
Meas./Sim.	Meas.	Sim.	Meas.	Sim.	Meas.	Sim.	Meas.	Sim.
Max. (°)	2.29	3.08	1.16	2.24	3.52	4.25	3.01	2.80
Std dev. (°)	0.49	0.79	0.25	0.45	0.83	1.13	0.67	0.56
Skewness	-0.06	-0.04	-0.04	-0.22	-0.38	0.34	-0.45	0.51
Kurtosis	0.05	0.41	-0.87	0.93	0.77	1.35	0.93	2.14

Table II: Moments of the measured and simulated data.

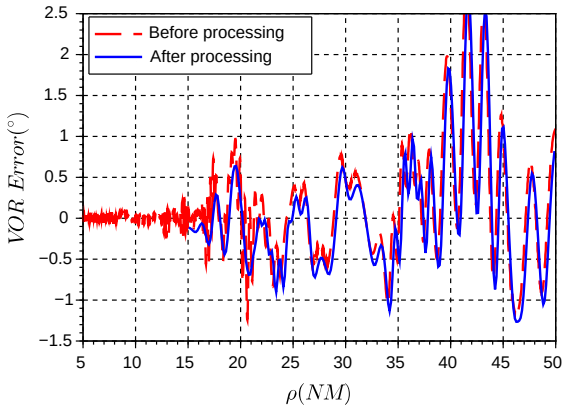

Figure 11: Simulated VOR error before and after processing with respect to distance in the presence of the wind turbines (Nov. 2012) for $\varphi = -10°$.

haviour of the measured errors are of the correct order of magnitude despite the noisy environment (vegetation, high voltage line) not accounted in the simulation, the PEPO method is considered successfully tested. Yet, comparisons with other measurements in a less noisy environment would be useful for a definitive validation. The computation time is 13 minutes for this scenario on a standard desktop computer.

IV. Investigation on the Simulation Results

In this section, complementary simulations are performed to show that the differences between the measurements with the rotor-blades (November 2012) and without the rotor-blades (July 2012) is due to the change of trajectory. The mast of the wind turbines are also shown to be the major cause of the VOR error in this scenario. Indeed, the contribution of every part of the wind turbines to the VOR error can be isolated when the currents are calculated.

A. Influence of the Aircraft Trajectory on the Measurement

As shown in Figures 6 and 7, the trajectories are not exactly the same between the two measurement campaigns on a given azimuth. In order to quantify the influence of the trajectory variations between the two campaigns on the same azimuth, three simulations are performed along the azimuth $\varphi \approx -10°$. The resulting VOR errors are plotted with respect to distance in Figure 12 with the three following configurations:

- azimuths of the Nov. 2012 campaign and 3120 ft of altitude (green);
- azimuths of the July 2012 campaign and 3120 ft of altitude (blue);
- azimuths of the July 2012 campaign and 3180 ft of altitude (red).

Note that 3120 ft and 3180 ft are the mean altitudes for the two studied campaigns on the azimuth $\varphi = -10°$.

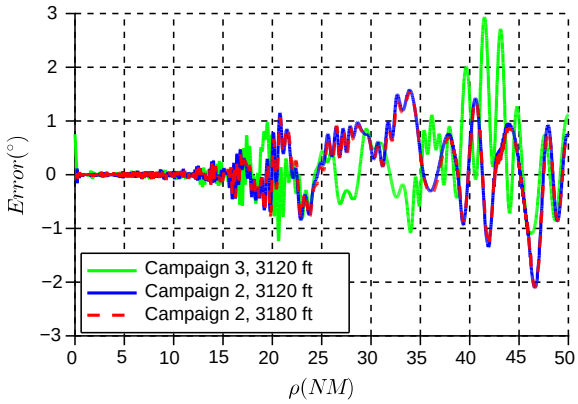

Figure 12: Simulated VOR error (°) due to the wind turbines for the aircraft azimuth of the two campaigns (around $\varphi = -10°$) and for two different altitudes.

The azimuth variation between the two campaigns has much more influence than the altitude variation. Indeed, the red and blue plots in Figure 12 coincide whereas the simulations performed with the same altitude but different azimuths (in green and blue) lead to differences up to 1.5° on the envelop. The oscillation period of the error (40-45 NM) is also modified. In conclusion, the knowledge of the azimuth of the receiver during the measurement is critical.

B. Quantification of the Contribution of Each Part of the Wind Turbines

The contribution to the VOR error of each component of the obstacles can be isolated during the calculation of the currents. The scattering from the blades and the hubs of the wind turbines is studied in this section. The VOR error simulated on azimuth $\varphi = -10°$ due to the hubs and blades only is plotted in Figure 13. The blue plot and the red plot correspond to hubs oriented as during the flight inspection measurement and facing West, respectively.

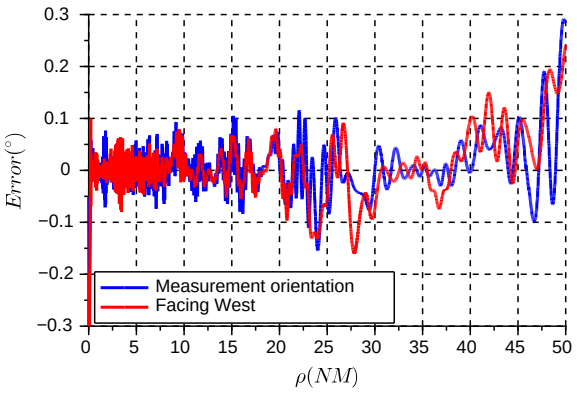

Figure 13: Simulation results of VOR error (°) due to the wind turbine hubs and blades for $\varphi = -10°$.

First, the blades and the hubs add an error smaller than $0.3°$. This is weak compared to the $1°$ total error in the area 45-50 NM. Therefore, the differences between the VOR error measured during the two campaigns are not due to the rotor-blades but to the trajectories mainly. Second, the VOR error variation when the rotors change of orientation is negligible, less than $0.05°$. So, the orientation of the rotor is unimportant in such a simulation scenario.

In conclusion, the PEPO method can be used to discriminate the contribution to the VOR error of the different scatterers. The influence of the various parameters impacting the VOR error can also be highlighted. Here, far from the VOR station (more than 15 NM), the masts are the main contributors to the error. The orientation of the rotor is shown to be a non-essential information for the VOR error simulation in that scenario.

V. Conclusion

The PEPO method used to simulate the VOR error due to the environment has been presented in this paper. The methods used for the propagation (PE) and the scattering (PO) computations have been individually exposed. The hybridisation technique between these two methods has been presented. The incident field considered as a plane wave on each facet allows a fast computation of the field radiated by the PO currents.

A confrontation with measurements has been presented with the CVOR of Boulogne-sur-Mer and nine wind turbines. The results show that the method is able to compute the VOR error due to complex obstacles such as wind turbines with a good accuracy and with a simulation time of about 13 min. The maximum error as well as the statistical properties (standard deviation, skewness, and Kurtosis) of the simulations are shown to be of the same order as for the measurements. Differences in the maxima are weaker than $1.1°$ with standard deviation differences smaller than $0.3°$. Kurtosis and skewness differences are less than 2 between measurements and simulations, which denotes similar behaviours. Considering the high variability of the VOR error with the position of the scatterers, the PEPO method is successfully tested. It should be compared to other measurements in simpler configurations to confirm the validation.

Finally, the method can also be used to discriminate the contributions of several obstacles or of their components in the VOR error. The hubs and blades influence are shown to be weaker than the masts influence for the studied scenario.

The PEPO method can be used preliminary to flight inspections to point to areas where the VOR system is the most impacted by a wind farm. This can also be useful to assist projects such as wind farm and buildings erections. The method could be improved for other kinds of scatterers. For example edge diffraction could be implemented to accurately consider the building influence. The method could also be improved by taking into account the relief between the scatterers and the aircraft.

Acknowledgement

The authors would like to thank the French Air Navigation Service Provider (DSNA/DTI) and the French civil aviation university (ENAC) for the founding.

References

[1] C. A. Balanis, *Advanced Engineering Electromagnetics*, 2nd ed. John Wiley & Sons, 2012.

[2] "European guidance material on managing building restricted areas," International Civil Aviation Organization (ICAO), Tech. Rep. EUR DOC 015, Novembre 2015, 3rd edition.

[3] S. Odunaiya and D. Quinet, "Calculations and analysis of signal processing by various navigation receivers architectures," in *The 23rd Digital Avionics Systems Conference, DASC 04.*, vol. 1, Oct 2004, pp. 1.D.1–11–13.

[4] C. Morlaas, M. Fares, and B. Souny, "Wind turbine effects on VOR system performance," *IEEE Transactions on Aerospace and Electronic Systems*, vol. 44, no. 4, pp. 1464–1476, 2008.

[5] D. de la Vega, C. Fernandez, O. Grande, I. Angulo, D. Guerra, Y. Wu, P. Angueira, and J. Ordiales, "Software tool for the analysis of potential impact of wind farms on radiocommunication services," in *IEEE International Symposium on Broadband Multimedia Systems and Broadcasting (BMSB)*, June 2011, pp. 1–5.

[6] A. Calo Casanova, M. Ramon, L. de Haro y Ariet, and P. Blanco-Gonzalez, "Wind farming interference effects," in *5th IEEE International Multi-Conference on Systems, Signals and Devices*, July 2008, pp. 1–6.

[7] ITU, "Assesment of impairment caused to television reception by a wind turbine," ITU-R BT 805, Tech. Rep., 2010.

[8] J. Fernandes, L. Correia, C. Alves, L. Pissarro, and M. Teixeira, "Assessment of wind turbines generators influence in VOR aeronautical navigation systems," in *IEEE Antennas and Propagation Society International Symposium (APSURSI)*, July 2014, pp. 709–710.

[9] F. Pérez Fontán, D. Marote, A. Mayo, B. Sanmartin, A. Castro, and J. J. Navarro, "Assessing multipath induced errors in VOR systems using ray-tracing techniques in combination with detailed terrain databases," in *14th International Flight Inspection Symposium (IFIS)*, June 2006, pp. 91–96.

[10] I. Gonzalez, L. Lozano, J. Gomez, A. Tayebi, I. Etayo, and M. Catedra, "Analysis of the scattering field of wind turbine using rigorous and asymptotic techniques," in *the Fourth European Conference on Antennas and Propagation (EuCAP)*, April 2010, pp. 1–4.

[11] C. Morlaas, A. Chabory, and B. Souny, "Propagation model for estimating VOR bearing error in the presence of windturbines – Hybridisation of parabolic equation with physical optics," in *the Fourth European Conference on Antennas and Propagation (EuCAP)*, April 2010, pp. 1–5.

[12] A. Calo Casanova, P. Pathak, and M. Calvo Ramon, "Modeling windmill interference via hybrid parabolic equation and equivalent current approximation methods," in *International Conference on Electromagnetics in Advanced Applications (ICEAA)*, Sept 2011, pp. 275–278.

[13] L. Claudepierre, R. Douvenot, A. Chabory, and C. Morlaas, "Assessment of the shadowing effect between windturbines," in *the 9th European Conference on Antennas and Propagation (EuCAP)*, April 2015, pp. 1–4.

[14] ——, "Influence of the lightning protection of blades on the field scattered by a windturbine," in *the 9th European Conference on Antennas and Propagation (EuCAP)*, April 2015, pp. 1–5.
[15] J. A. Stratton, *Electromagnetic Theory*, ser. IEEE Press. John Wiley & Sons, 2007.
[16] M. Levy, *Parabolic Equation Methods for Electromagnetic Wave Propagation*, ser. IEE electromagnetic waves 45. IET, 2000.
[17] J. R. Kuttler and D. G. Dockery, "Theoretical description of the parabolic approximation/Fourier split-step method of representing electromagnetic propagation in the troposphere," *Radio Science*, vol. 26, no. 2, pp. 381–393, 1991.
[18] G. D. Dockery and J. R. Kuttler, "An improved impedance-boundary algorithm for Fourier split-step solutions of the parabolic wave equation," *IEEE Transactions on Antennas and Propagation*, vol. 44, pp. 1592–1599, 1996.
[19] M. A. Leontovich, *Investigations of Propagation of Radio Waves*. Moscow, U.S.S.R.: Academy of Sciences, 1948, ch. On the approximate boundary conditions for electromagnetic fields on the surface of well-conducting bodies, pp. 5–20.
[20] A. R. Miller, R. M. Brown, and E. Vegh, "New derivation for the rough-surface reflection coefficient and for the distribution of sea-wave elevations," in *IEE Proc. H Microwaves, Optics and Antennas*, vol. 131, 1984, pp. 114–116.
[21] S. Laybros, P. F. Combes, and H. J. Mametsa, "The "very-near-field" region of equiphase radiating apertures," *IEEE Antennas and Propagation Magazine*, vol. 47, pp. 50–66, 2005.
[22] S.-W. Lee and R. Mittra, "Fourier transform of a polygonal shape function and its application in electromagnetics," *IEEE Transactions on Antennas and Propagation*, vol. 31, pp. 99–103, 1983.
[23] G. T. Ruck, D. E. Barrick, W. D. Stuart, and C. Krichbaum, *Radar Cross Section Handbook: Volume 1*, G. T. Ryck, Ed. Peninsula Publishing, 2002.
[24] D. L. Sengupta, "Theory of scalloping amplitude errors in standard VOR bearing indications," *IEEE Transactions on Aerospace and Electronic Systems*, vol. AES-11, pp. 86–93, 1975.
[25] ITU, "Electrical characteristics of the surface of the earth," ITU-R P.527-3, Tech. Rep., 1992.
[26] G. Apaydin and L. Sevgi, "The split-step-Fourier and finite-element-based parabolic-equation propagation-prediction tools: Canonical tests, systematic comparisons, and calibration," *IEEE Antennas and Propagation Magazine*, vol. 52, pp. 66–79, 2010.
[27] A. Stuart and J. Ord, *Kendall's Advanced Theory of Statistics. Volume I: Distribution Theory*, 5th ed. London: Griffin and Co., 1987.
[28] A. Field, *Discovering Statistics using SPSS*. London: SAGE, 2009.

Ludovic Claudepierre Ludovic Claudepierre was born in CondÃľ-sur-l'Escaut, France, in 1990. He received the engineer degree from the ENSEEIHT (École Nationale SupÃľrieure dâĂŹĂĽlectrotechnique, ÃĽlectronique, Informatique, Hydraulique et TÃľlÃľcommunication) in Toulouse, France, in 2012. He received the Ph.D degree from the Toulouse University (France) in electromagnetism and high-frequency systems. His research topics are propagation, electromagnetic modelling, and wind-turbine interference on radar and VHF systems.

Rémi Douvenot was born in Chartres, France, in 1982. He received the engineer degree from the ENAC (French National Civil Aviation School), the M.Sc. from Toulouse University, France, in 2005, and the Ph.D. degrees in electrical engineering from Nantes University, France, in 2008. His Ph.D. was on refractivity from clutter. In 2009, he worked with the Laboratoire des Signaux et Systèmes (L2S), UMR (SUPELEC - CNRS - Univ Paris-Sud) on non-destructive testing using eddy-currents. Since 2011, he has been lecturer in electromagnetics with TELECOM/EMA research group, ENAC in Toulouse, France. His main research interests are the theory of wave propagation and its applications to radar and air transport devices.

Alexandre Chabory received the M.Sc. degree in electronic engineering from the French Civil Aviation University (ENAC), Toulouse, France, in 2001. He received the Ph.D. degree in electromagnetics from Paul Sabatier University, Toulouse, France, in 2004.

From 2004 to 2007, he was a Postdoctoral Scientist with the Eindhoven University of Technology (TU/e), Eindhoven, The Netherlands. Since 2007, he has been an Assistant Professor with the Electromagnetics and Antennas Research Group, Telecom Laboratory, ENAC, Toulouse, France. Since 2012, he has been the head of this group. His research interests include electromagnetic theory and modeling, mainly for aeronautical applications.

Christophe Morlaas received the Ph.D. degree in electronics from ISAE-SUPAERO ("Institut Supérieur de l'Aéronautique et de l'Espace") in 2000. He hold a system engineer position in spatial programs until 2002. Since then, he is an assistant professor with the Electromagnetics and Antennas Research Group of the Telecom lab of ENAC. His research interests include aeronautical communication and navigation systems, electromagnetic modelling, propagation models, and antenna design.